THE PENNSYLVANIA STATE UNIVERSITY
SCHREYER HONORS COLLEGE

DEPARTMENT OF ENGINEERING SCIENCE AND MECHANICS

DEVELOPMENT OF A LOW-FIELD ELECTRICALLY DETECTED MAGNETIC RESONANCE SYSTEM TO OBSERVE PERFORMANCE LIMITING DEFECTS IN CdTe/CdS SOLAR CELLS

ERIK T. SHAW
SPRING 2014

A thesis
submitted in partial fulfillment
of the requirements
for a baccalaureate degree
in Engineering Science
with honors in Engineering Science

Reviewed and approved* by the following:

Patrick M. Lenahan
Distinguished Professor of Engineering Science and Mechanics
Thesis Supervisor

Barbara A. Shaw
Professor of Engineering Science and Mechanics
Honors Advisor

Judith A. Todd
P.B. Breneman Department Head Chair
Professor, Department of Engineering Science and Mechanics

* Signatures are on file in the Schreyer Honors College.

ABSTRACT

Electrically detected magnetic resonance (EDMR) has proved to be a valuable analytic tool for the characterization of defects in semiconductor devices. By measuring small changes in current in the device, EDMR has much higher defect sensitivity than conventional electron paramagnetic resonance (EPR). Low-field EDMR is a new technique that has shown promise in defect characterization. Conventional EPR has very low sensitivity at low magnetic fields, but this is not a problem with EDMR. In fact, making EDMR measurements at low magnetic field may have benefits in signal strength. We developed an EDMR system from the ground up. This system consists of several subsystems, which will be discussed in depth. The completed system is capable of producing a reproducible and well calibrated magnetic field ranging from -150 to +150 Gauss, a variable modulating field, and an applied RF power. The goal was to successfully show that the low-field EDMR system was operational, and then use it to observe spin dependent recombination (SDR) in various devices, most notably CdTe/CdS solar cells from the National Renewable Energy Lab (NREL). We will first discuss the theory of operation of the system and some background on CdTe/CdS solar cells, EDMR, and EPR of CdTe. Then, we will give a detailed description of all the equipment used in the EDMR set up and how the subsystems function. We were able to successfully achieve a zero field response for a well characterized 4H SiC DMOSFET, and then possibly achieved a zero field spectrum for CdTe/CdS under forward bias. The results will be analyzed and then further areas of research will be discussed.

TABLE OF CONTENTS

List of Figures iii

List of Tables iv

Acknowledgements v

Chapter 1 Introduction 1

- Material Characteristics 2
- Electrically Detected Magnetic Resonance Imaging 4
- Downsides 5
- Conclusions 7

Chapter 2 Background 9

Chapter 3 Experimental Setup 14

- Main Helmholtz Coils 15
  - Programming Current Ramp 15
  - Main Helmholtz Coils 17
- Modulation Helmholtz Coils 19
- Sample Biasing, Signal Amplification and Averaging 21
  - Sample Mounting 21
  - Sample Holder 24
  - Sample Biasing 25
  - Signal Amplification 26
  - Signal Averaging 27
- RF Power 28

Chapter 4 Results 31

- CdTe/CdS I-V Curve 31
- 4H SiC DMOSFET Low-field EDMR Results 32
- CdTe/CdS Low-field EDMR Results 34

Chapter 5 Discussion 37

- Problems Encountered 37
- Future Work 40

- Appendix A Calculations & Programs 42
- Appendix B System Components 44
- References 45

LIST OF FIGURES

Figure 2.1: Grain structure schematic 10

Figure 3.1: EDMR system schematic 14

Figure 3.2: Experimental setup 15

Figure 3.3: Helmholtz coil diagram 18

Figure 3.4: Qualitative display of modulation field 19

Figure 3.5: Importance of modulation amplitude 20

Figure 3.6: Sample preparation schematic 22

Figure 3.7: Sample preparation 23

Figure 3.8: Early jig designs 24

Figure 3.9: Final jig design, front (left) and back (right) 25

Figure 3.10: Qualitative diagram for calculating Q 29

Figure 4.1: I-V curve characteristics for CdTe/CdS sample 31

Figure 4.2: First characteristic spectra 32

Figure 4.3: Spectra after further system optimization 33

Figure 4.4: Fully optimized signal response 33

Figure 4.5: Possible CdTe/CdS zero-field response at 75Hz 34

Figure 4.6: Possible CdTe/CdS zero field response at 100Hz 35

Figure 4.7: Zoomed in CdTe/CdS response at 100Hz 35

Figure 5.1: Comparison of signal response using two different current pre-amps 39

LIST OF TABLES

Table 1: System settings at 5 Gauss mod.....43

Table 2: System component details 44

ACKNOWLEDGEMENTS

I would like to thank Jim Ashton and Dan Galante for helping me put together this low-field EDMR system. Thank you to Colin McKay and Chris Perini for designing and building the magnet.

I would like to thank graduate students Mike Mutch, Mark Anders, and DJ McCrory for their support and teaching me what I needed to know about EDMR, biasing, and the various computer programs. Thank you to Liam Young as well for helping with the sample mounting.

I would like to thank Dr. Lenahan for his advice and being instrumental to getting the system to work. Thanks for always taking the time to explain the physics behind EDMR and guiding me in the right direction. Also, thank you for editing my drafts and helping me finalize my thesis.

Lastly, I would like to thank my best friend, Alexandra Beebe, and my parents for their support of my project.

Chapter 1

Introduction

Sustainable energy production is becoming increasingly important to meet the world's energy demands. New technologies are being developed and refined as scientists and engineers work towards ways to replace fossil fuels. Using the sun as an energy source has significant benefits and has been the source of numerous research studies. Energy from the sun is sustainable and completely renewable. This energy comes from photons emitted by the sun, with 120,000 TW hitting the Earth's surface. Projected energy needs in 2030 could be met by covering just 0.8% of land with 10% efficient panels [1].

The majority of these modules today are based around silicon architecture. This technology, however, has limits in adaptability and price, and thus new materials have shown significant potential to replace silicon as the semiconductor in photovoltaics.

Cadmium telluride has emerged as one of the best candidates to replace silicon. CdTe has a band gap of 1.44 eV at room temperature, which corresponds well to the theoretical Shockley-Queisser limit for maximum efficiency, which is above 33% [2]. Thin-film solar cells based on a p-n junction of CdS/CdTe are projected to be cheaper and versatile than silicon.

Currently, silicon prices have fallen drastically and thin-film technology has struggled to keep raising efficiencies while lowering manufacturing costs. The big problem with CdTe based solar cells is that their efficiencies are lower than silicon. The

problem with efficiency is closely related to recombination centers in the device. Recombination centers are mostly material defects, like dangling bonds or impurity atoms. These centers trap electrons, limiting current flow and overall power output. Identifying these centers is imperative to understanding and correcting the defects. The defect concentration is so low that there are few analytic techniques that can be used to characterize this phenomenon.

One potential answer is to analyze the material using electrically detected magnetic resonance imaging. EDMR is a technique that is being effectively used on semiconductors like SiC, and has applications for CdTe. Unique properties of this technique allow for a much higher magnitude of sensitivity, translating to detecting smaller quantities of defects. Results from EDMR analyses could help to understand what defects are present in CdTe/CdS, and whether or not they limit performance.

Material Characteristics

Since a need for sustainable forms of energy was first realized, solar technology has promised to be a viable solution. The resulting cost of the technology, however, has always been the limited factor and prevented mainstream adoption. CdTe technology has been rapidly advancing, and has several benefits over traditional technologies.

Cadmium telluride semiconductors have a bandgap of about 1.5 eV. This energy corresponds to the wavelength of light that CdTe can absorb. Because of the sun's distribution of different wavelengths of photons and quantum properties of semiconductors, a theoretical maximum efficiency exists, an efficiency which is much less than 100%.

According to the Shockley-Queisser limit for maximum efficiency, the ideal bandgap is approximately 1.2-1.5eV [2].

CdTe has a bandgap in this region, and as such has the highest potential to achieve maximum efficiency for a single-junction solar cell. In reality, this efficiency is much less because of losses at the quantum level and at material junctions. However, this theoretical efficiency can be even higher using materials with different bandgaps to create multi-junction solar cells, as this allows the maximum range of the sun's light to be absorbed. For cost-effectiveness, a simple CdTe/CdS cell provides the best economical compromise between efficiency and performance.

Another important consideration for a doped semiconductor to be used in solar cells is their effectiveness at elevated temperatures. Electronics, like computer processors, operate better cold. Under direct sunlight, solar panels will experience a rise in temperature. As this is often when a solar cell will produce the most electricity, it is imperative that the materials used can still perform with changes in temperature.

Studies have shown that CdTe is indeed effective even at high temperatures. A study found that under thermal straining at levels a PV panel would experience under direct sunlight, CdTe outperformed traditional silicon modules [3]. This is promising and further supports further research into CdTe solar cells.

Additional properties of CdTe make it effective even at small thicknesses. Current thin-film techniques allow for modules that use 1-2% of the material that a traditional silicon design would need for the same performance level [3]. Thin-films can require specialized techniques, like molecular beam epitaxy (MBE), and specialized equipment and

clean rooms. CdTe, however, can be produced in a much less clean environment. These properties and production capabilities allow CdTe to be manufactured at higher volumes for much cheaper than other specialized materials.

Electrically Detected Magnetic Resonance Imaging

A large part of the efficiency limitations in CdTe solar cells is a result of material defects in the semiconducting material. There are two techniques being used to analyze these defects, electrically detected magnetic resonance (EDMR) and electron spin resonance (ESR). These techniques work well for not just CdTe, but for thin film solar cells based on II VI semiconductor systems.

ESR is a sensitive technique, with sufficient analytical power to be able to provide accurate renditions of the atomic structure at an atomic level, as well as the chemical nature of the defect. EDMR is a method where the electronic measurement— voltage, current, or capacitance—is used to obtain the ESR measurement [4]. This method provides much more resolution and can provide greater detail than conventional ESR techniques. A measurement using EDMR, called spin dependent recombination (SDR), is the ideal method of analyzing defects. This method allows for an analysis of the deep level defect centers, which are the areas that most limit carrier lifetime and thus efficiency.

The reason why CdTe is such a good candidate for analysis using magnetic resonance is that it contains nuclei that are naturally magnetic. Cadmium contains two magnetic isotopes, 111i and 113. These isotopes have a spin quantum number of ½ and

are about 12% naturally abundant [4]. Tellurium, also has two magnetic isotopes, 123 and 125. These magnetic nuclei also have a spin number of ½, but are only 8% abundant. The fact that cadmium and telluride both have magnetic nuclei with spin numbers of ½ makes the analysis much easier. The resonance states for these nuclei yield only two conditions: ± ½. This means that when the magnetic field used in the analysis is applied, the nuclei can either align with or against the magnetic field. This gives a simple two peak pattern, and provides accurate results for each defect site.

There are two main problems using conventional ESR techniques. The first is that it is difficult to separate out only the defects which have the biggest impact on device efficiency. The second is that the defect resolution using ESR is low. This means that analysis of a material with orders of magnitude fewer defects than can be analyzed would not yield useful measurements, because of the experimental limitations. Using EDMR to measure SDR, these problems can mostly be addressed and overcome, thus expanding the scope and capabilities of magnetic resonance.

Downsides

While there is significant potential for CdTe use in the industry, the material has several unique issues compared to silicon. These issues could have significant impact on the production capabilities and implementation safety. The first downside for CdTe is the availability of the two elements, cadmium and tellurium. Whereas silicon is one of the most abundant elements on Earth, the supply of tellurium is limited. This could easily affect production rates. The other key downside to CdTe is the cadmium is a toxic heavy

metal. Groundwater contamination is a possibility during the lifetime of a panel, as is environmental damage during fabrication.

Cadmium is a relatively abundant material, but tellurium is not nearly as abundant. Tellurium is a rare earth element that is found only on levels from 1-5 parts per billion naturally on Earth [5]. The majority of commercial tellurium is a byproduct of the manufacturing of copper, lead and gold. Currently, the supply and production of tellurium is limited enough to cause significant limitations in the production of telluride-based cells, especially as these cells see increased use. Researchers are currently studying undersea ridges, which are rich in tellurium content [5]. These ridges, if they could be mined and economically processed, have to potential to significantly increase the availability and supply of tellurium. If this process could be made hyper-efficient and feasible by advances in marine mining technology, this could be a huge factor in the cost of production of CdTe films. Reducing the buy-back period is a big factor in marketing and the sales of solar panels, especially with residential cases. A rise in the tellurium supply, driving the price of the raw materials used in CdTe solar cell fabrication down, could provide a significant economic boost and increase the affordability of solar cell technology.

The factor in the production of CdTe films that has the biggest impact on the environment is the toxicity of cadmium. Cadmium is a toxic heavy metal, and is one of the most deadly materials known to humans. Cadmium telluride can be toxic as well, especially if ingested, powdered CdTe is inhaled, or if the material is mishandled [5]. Numerous studies are attempting to determine the extent of the contamination and

chemical hazard risk associated with processed cadmium. Specific studies have been sponsored by First Solar to address this risk.

One environmental study was performed by V.M. Fthenakis at a PV environmental research center in New York. In terms of simple emissions, PV cells made from CdTe will emit the least quantity of harmful air pollution because the cells require the least energy to manufacture [6]. If energy to power the grid was exclusively generated by photovoltaics, about 90% of all emissions could be reduced [6]. It is clear that CdTe based solar cells have advantages , especially with low lifecycle emissions, and that widespread use would be beneficial to the environment.

The study also followed the amount of heavy metals released during production and operation. Fthenakis concluded that under standard operating procedures, there are no cadmium emissions to air, soil, or water [6]. Cadmium emissions under extreme situations like fires or broken panels were negligible [6].

This study, among others, shows that cadmium toxicity is a concern, yet when proper procedures are employed, there is a reduced risk, especially once the panels are produced. During fires and high heat failure, the glass of the panels actually fuses together, trapping the CdTe material and thus further reducing contamination risk.

Conclusions

CdTe has seen a significant increase in use recently. This is mainly due to several properties of CdTe that make it a particularly suitable material for solar cell application. CdTe based PV modules can also be manufactured cost-effectively, reducing consumer

buy-back periods. The main problem with this technology is reduced efficiency levels—especially compared to theoretical values—but even more importantly with competing silicon-based technologies. Because of the element cadmium that makes up CdTe, there is a risk of negative environmental impact. Studies have been done that have shown that even under complete failure, the panels remain stable and do not leach toxic amounts of cadmium into the environment. PV panels made using CdTe/CdS actually have the smallest environmental footprint of any technology in use today. CdTe based solar cells are an excellent choice for a photovoltaics, and techniques like EDMR continue to help refine this industry and advance the technology.

Chapter 2

Background

One of the best analytical tools for semiconductor analysis is magnetic resonance. Electron paramagnetic resonance studies of CdTe material have shown the ability to identify several defects in the microstructure. EDMR has further advantages of higher defect resolution and the ability to test fully fabricated devices.

The principles of EDMR are well understood [7]. In a p-n junction semiconductor there is a depletion region at the junction where there is a non-equilibrium of electrons and holes. In order for the system to regain equilibrium, recombination or generation will occur. Recombination occurs when electron-hole pairs are eliminated, while generation is where the electron-hole pairs are generated. Recombination and recombination current is what is studied using EDMR.

Recombination can only occur when an electron spin and the unpaired spin of the recombination site are opposite. If both electron and site have the same spin, the transition is forbidden and will not occur. When the magnetic resonance conditions are met, either the electron's or site's spins are altered, or both spins are altered. This condition is defined by the following equation:

$$h\nu = g\mu_B B$$

where h is Planck's constant, ν is the applied frequency, g is the g tensor, μ_B is the Bohr magneton, and B is the applied magnetic field.

The altering of spins can make a previous forbidden transition allowable. The new recombination events alter the conductivity of the material. This effect can be quantified by measuring the current change in the device. The benefit of EDMR is the sensitivity. Typically, the change in current is sufficiently large that the defect resolution of EDMR is much higher than conventional ESR, typically 100 times or much more [7].

Recombination centers can be a variety of material defects. Figure 2.1 shows a representative schematic of a typical CdTe/CdS cell, much like the sample that will be

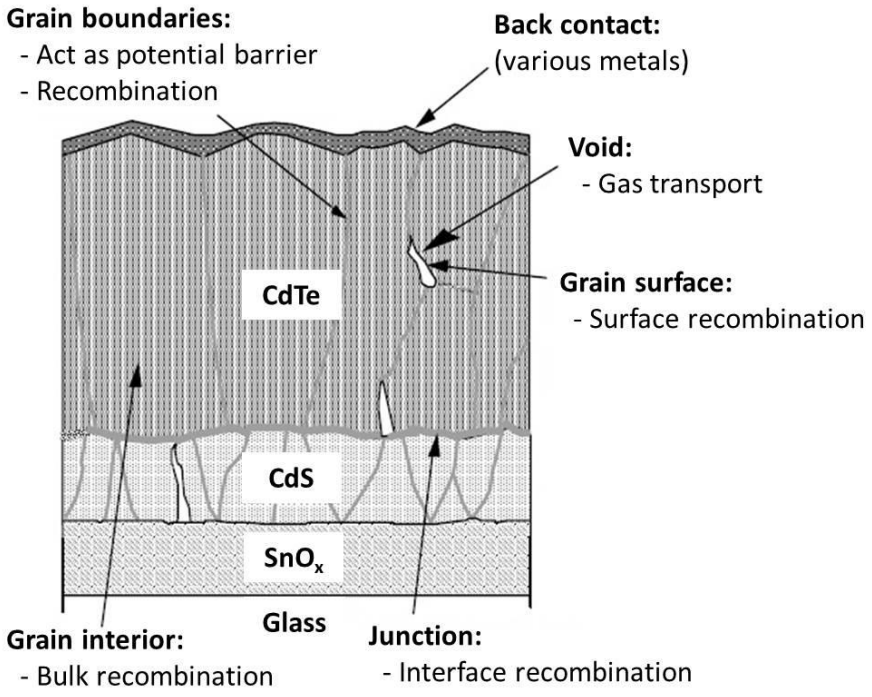

Figure 2.1: Grain structure schematic (adapted from [8])

tested. There are many places where recombination can occur, including bulk recombination, surface recombination at grain surfaces, and interface recombination. Some defects have already been characterized using EPR.

EPR is a more general technique where electron spins are flipped and the subsequent response gives information about the location of the electrons. EPR has been used to identify various dopants like chromium and manganese ions, cadmium vacancies, and more. A recent study has shown conclusive evidence that EPR has the analytic power to observe defect centers in CdTe/CdS solar cells [9].

A study done by a research team in Poland identified chromium ions in the CdTe crystal. The team used a Bruker ESP-300 spectrometer and made the measurements at room temperature and at X-band (9.6 GHz) [10]. The EPR spectra showed a dependence on angular orientation. The results of the EPR spectra indicated that the defect was a Cr^{3+} ion that had taken the place of a cadmium atom [10].

The absence of a cadmium atom in the CdTe microstructure has been studied using EPR as well, and labeled as an A center. Using the same Bruker 300 spectrometer, measurements were made this time at 25K using helium as a coolant [11]. The defect was detected in its single negative charge state, and it was shown that it has trigonal symmetry. Hyperfine interactions from the spectra show that the hole is localized on a Te atom [11].

A study done in Germany showed a new defect center that was discovered after irradiation of CdTe with neutrons. The defect consists of a Cd vacancy and either a donor on an adjacent Te or and impurity isoelectronic to Te [12]. This is a variation of an A center, and the defect was labeled XA.

A Te vacancy, also called an F center, was observed by a study done in Europe. An F center defect is an isolated anion vacancy. The defect was characterized with a

isotropic g value of 2.000±0.001 and hyperfine interactions showing it was surrounded by four Cd atoms [13].

Titanium and vanadium doped CdTe signals have been observed using optically detected magnetic resonance (ODMR) and EPR [14]. EPR results show that Ti ions are either in Ti^{2+} or T^{3+} states, while V ions are only in the V^{3+} state [14].

Lead, tin and germanium doped samples were studied using EPR in 1985. Spectra were obtained for each ion, with all tests undergone at X-band and 20K [15].

Using a variation of EPR involving spin-flip Raman scattering (SFRS), researchers have been able to use optically detected spin resonance techniques to observe Mn^{2+} $3d^5$ spin level ions in CdTe [16]. The line shape was dominated by hyperfine interactions, leaving the resonant intermediate state to be characterized by a free or weakly localized exciton [16].

Annealing CdTe in a $CdCl_2$ based environment has shown to significantly improve device performance [17]. Adding the Cl to the lattice will add Cl as a substitute for a Te vacancy, or F center. This effect has been documented by EPR studies [18], [19]. In a preliminary study, spectra for Cl, In, and Al doped CdTe were observed under photon illumination at 12K [18]. It was concluded that these elements were shallow donor defects [18]. In a follow-up study, EPR was done on Cl doped CdTe after varying degrees of heat treatment [19]. The results of this study showed a signal dependence on annealing temperature.

Although there has been no direct evidence that the addition of copper to the contacts increases recombination in CdTe solar cells, Cu has been shown to limit performance, particularly when the device is stressed [20]–[22]. A small amount of Cu is

used to improve back contact properties. Although no EPR results have been documented, Cu would be an atom to look for in an EDMR spectrum, particularly if the device is being thermally stressed.

There have been many EPR studies on doped, treated, and untreated CdTe. The studies summarized provide a background as to what to expect from the samples that will be tested and future samples produced using varying manufacturing techniques. Any features in the spectrum to be analyzed can be cross-referenced with the results of these studies to validate conclusions.

Chapter 3

Experimental Setup

A low field EDMR spectrometer requires the use of five different sub-systems. The first is the larger, multiple Helmholtz coils system, which provide calibrated and repeatable magnetic field sweeps from -150 to 150 Gauss. The second component is the pair of modulation Helmholtz coils, which help via lock-in detection help improve signal resolution. The third system is an RF power circuit, which makes up an oscillation magnetic field. The fourth system controls the semiconductor device biasing and signal

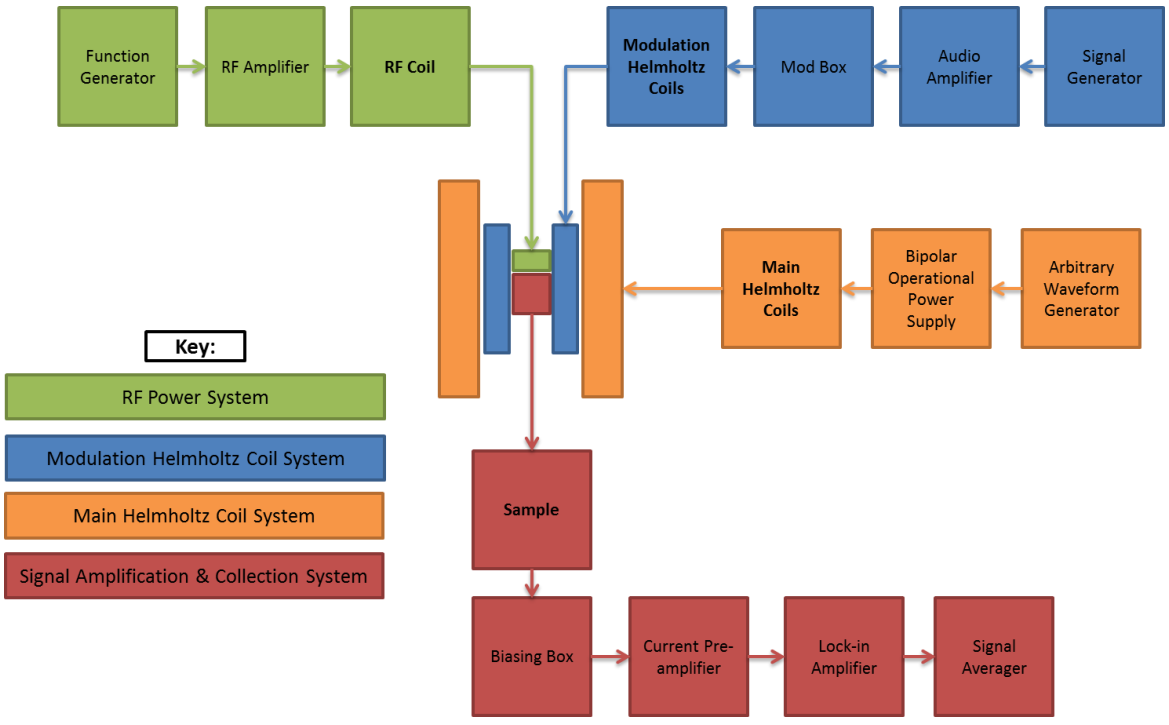

Figure 3.1: EDMR system schematic

amplification. The fifth component records and averages the resultant EDMR spectra. These systems must all work together, and optimizing them is important for achieving a reliable, high signal-to-noise measurement.

Figure 3.1 shows a schematic of the experimental setup, while Figure 3.2 shows the actual setup. Each system will be thoroughly discussed, and a comprehensive list of equipment will be given in Appendix B.

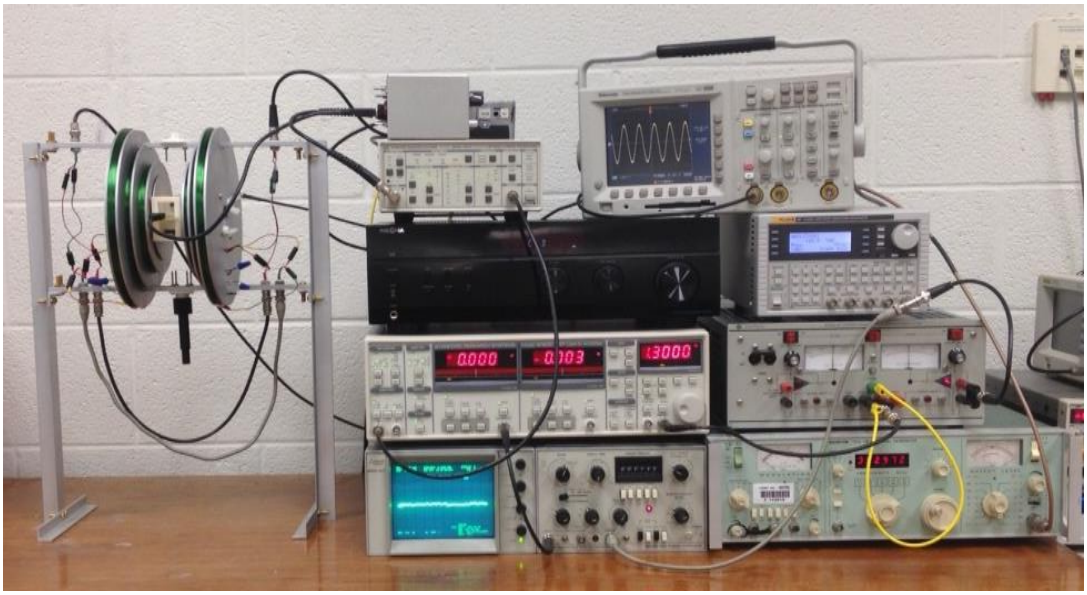

Figure 3.2: Experimental setup

Main Helmholtz Coils

Programming Current Ramp

The main Helmholtz coils are powered by a Kepco bipolar operational power supply. No computer or computer software is used in this set up, so the power supply had to be programmed in order to produce the correct current to power the Helmholtz

coils. The current programming was done using the current programming input on the Kepco supply.

The easiest way to program the current source was by using an arbitrary waveform generator. In order to get to 150 Gauss, 2 Amps of current needed to be applied to the magnet. Ideally, the power supply would sweep a current linearly from -2 Amps to 2 Amps, and then jump instantaneously back down to -2 Amps and run the sweep again. To achieve this, a ramp waveform was used. The amplitude of this wave dictated the amount of current supplied by the power supply. 20 Vpp coincided to 2 Amps while 10 Vpp produced 1 Amp. The period should be variable, optimized for the spectra you expect. For a full field sweep, we started with a period of 208 seconds, which allowed for a steadily increasing sweep as well as time for the signal averager to reset after each run. Later, these settings were modified to sweep through various fields as shown in Appendix B, Table 1.

The signal averager display was 10 divisions at a user-designated time per division. For a full-field sweep, the averager was set to 20.48 seconds per division, meaning that a full run recorded data for 204.8 seconds. After the 204.8 seconds, there was a delay in the signal averager, during which the device ended a run and then triggered and began another run. This delay meant that a period of more than 204.8 seconds had to be used in order for the runs to end correctly and then trigger and start again. After testing through trial and error as the exact delay time was unknown, a period of 208 seconds optimized the sweep. However, due to the reset delay the run ended prematurely and could apparently not record data after 204.8 seconds. This means that while the run started correctly at -2 A, the top range was only about 1.95 A. This issue

was only minor, and could be fixed by slightly increasing the magnetic field sweep time. In the near future, we will develop a more permanent fix by upgrading to a computer and using software to record data and program the current sweep.

The signal averager required a trigger input to correctly know when to begin a sweep. The trigger was set to the most negative slope, and the input was the just the arbitrary waveform that was used to input the current programming control. The negative slope setting enabled the signal averager to start each run at exactly the start of the waveform, which corresponds to -2A and -150 Gauss or another desired magnetic field amplitude.

Main Helmholtz Coils

The current output from the Kepco power supply went directly to the main Helmholtz coils. Helmholtz coils are essentially just an electromagnetic device that will produce a magnetic field. This magnetic field is useful for a number of reasons. It can effectively produce a nearly uniform field, which is very useful for the experiments we will be running [23]. The coils are designed using the governing equation:

$$B = \left(\frac{4}{5}\right)^{\frac{3}{2}} * \frac{\mu_0 nI}{R}$$

where B is the resultant magnetic field, μ_0 is the permeability of free space, n is the number of turns in each coil, I is the current through the coil, and R is the distance between the two coils. The coils are orientated as shown in Figure 3.3.

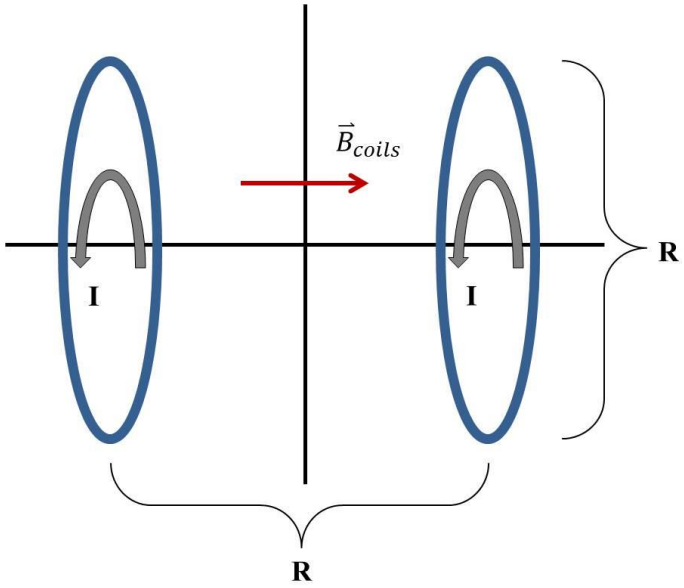

Figure 3.3: Helmholtz coil diagram

Each individual coil must be separated so that the distance between coinciding coils is exactly the radius of each coil. This is the dimension R shown in Figure 3.3. The current must also run in the same direction in each coil. Multiple coils can be used to increase the uniformity and also the magnitude of the magnetic field. The main field Helmholtz magnet design used had three sets of coils. One set of somewhat smaller modulation coils were included in the design to allow for lock-in detection.

Modulation Helmholtz Coils

The modulation coils provide an oscillating magnetic field on the order of a few Gauss. This oscillating field is complementary to the magnetic field from the main Helmholtz coils, and can significantly reduce signal noise with the use of lock-in detection. The magnetic field sweep is qualitatively illustrated in Figure 3.4.

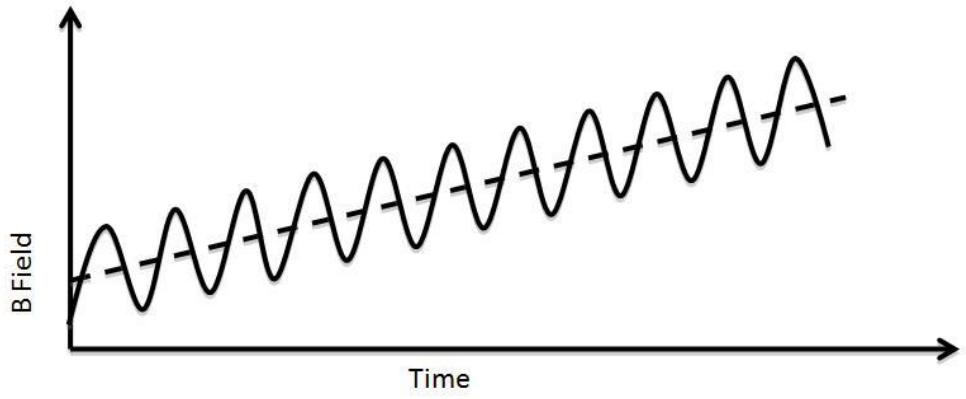

Figure 3.4: Qualitative display of modulation field [25]

The dashed line indicates the slowly varying magnetic field due to the main Helmholtz coils, and the solid sine wave indicates the sum of that field plus the modulation field. Although the diagram is greatly exaggerated, the principle of operation what is important.

The modulation field helps reduce noise when using a lock-in amplifier. The lock-in amplifier is phase and frequency sensitive, and can pick out the signal of interest and amplify it. The lock-in amplifier can be set to filter out any signal that is not at the phase and frequency set by the signal generator, thus reducing signal noise.

The modulation coils are driven by a signal generator, which outputs a sine wave at an audio frequency. This frequency can vary from 100 Hz to well beyond 10 kHz. Different frequencies can give you different signal amplitudes and signal widths. The amplitude of the sine wave should usually be directly proportional to the modulation field width; however, this is not always the case.

To achieve a sufficient drive current for the modulation coils, an audio amplifier was used. The audio amplifier amplifies the signal from the signal generator, and thus increases the mod field amplitude. This was important to achieving an optimal signal.

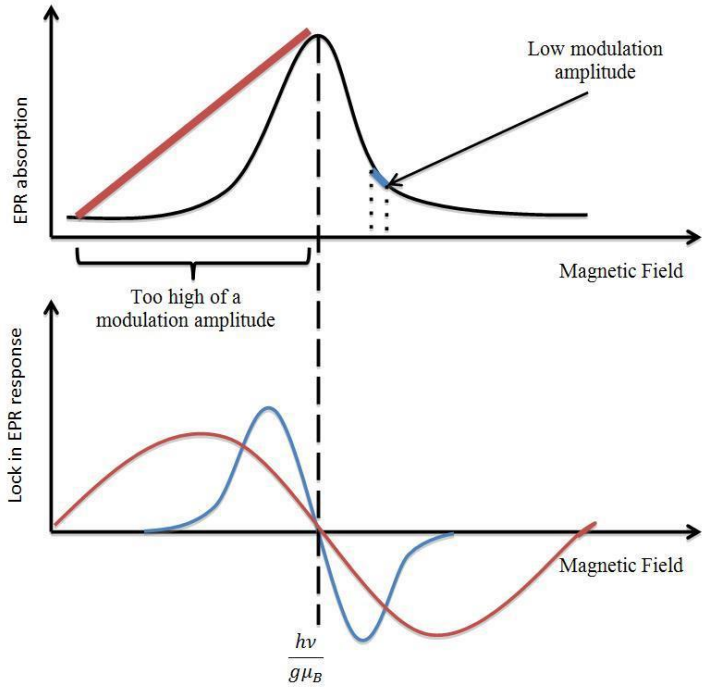

Figure 3.5: Importance of modulation amplitude [25]

There is always an optimum modulation amplitude. Modulating at too high or too low can distort the signal, an effect that can be qualitatively observed in Figure 3.5. In

our measurements, the amplitude required larger drive currents than could be generated without the use of an audio amplifier.

After the signal was amplified by the audio amplifier, the signal passed through a mod box. The mod box is just a circuit that had a 1Ω resistor, and a 10A fuse to protect mod coil circuit. The signal passed though the 1Ω resistor and then out to power the mod coils. This 1Ω resistance was used to allow direct voltage to ampere conversion for the modulation field drive current. The modulation field is proportional to the drive current in the mod coils. An oscilloscope could be connected to the mod box so the sine waveform driving the mod coils could be observed.

Sample Biasing, Signal Amplification and Averaging

Sample Mounting

The EDMR device samples were mounted on a custom circuit board and then placed in a specially designed sample holder. Because the solar cell samples are large relative to other EDMR samples undergoing testing, a somewhat more complex system was required to successfully mount and study the devices.

The PCB layout is simple and consists of four leads. The leads correspond to the source, drain, gate, and ground for other samples, mainly metal oxide semiconductor field effect transistors (MOSFETs). Because the solar cell devices only had two contacts, the two contacts were connected to the outside leads, leaving the other two leads unused.

The leads led to a USB adapter, which was soldered to the leads. When using the current preamp to bias samples, an additional USB to BNC adapter is required.

Mounting the sample proved to be very difficult. The devices were not glass encased, so they had to be mounted upside down. In order to have a sample sensitive to light, a hole had to be drilled through the PCB so that the active layer of the solar cell could be exposed to light. The light creates electron-hole pairs in the solar cells,

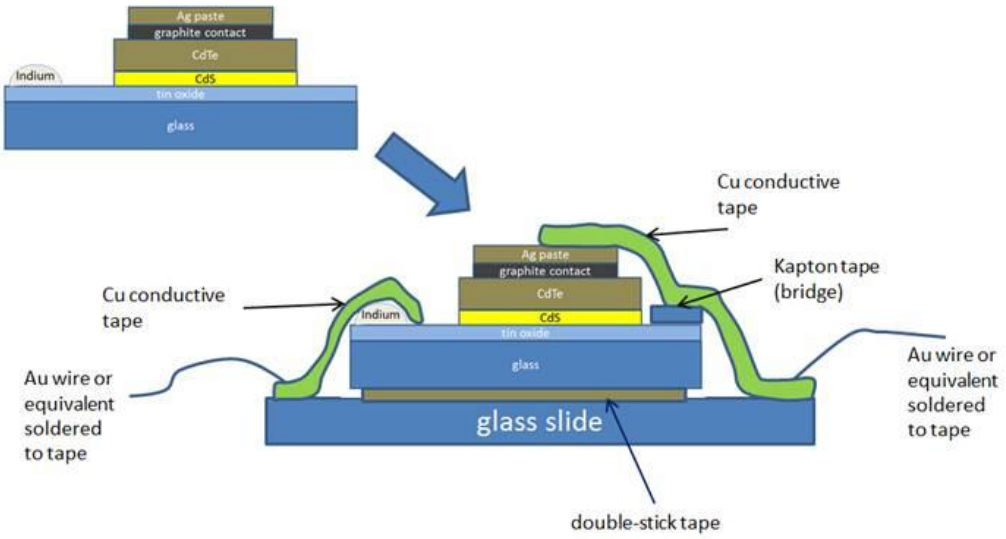

Figure 3.6: Sample preparation schematic

producing a current which may then be utilized in the resonance detection. The sample had exposed contacts: a front contact of indium and a back contact of silver paste. These two metal layers are exceptionally fragile, and thus could not be soldered. The first method that was used was suggested by Dr. David Albin of the National Renewable Energy Lab (NREL). A diagram of the proposed mounting scheme is shown in Figure 3.6.

This diagram shows how copper tape with conductive adhesive can be used to make electrical contact. Only a strip of copper tape is needed to attach the front indium contact, while insulating kepton tape is used to prevent a short when using the copper tape for the back contact lead. Figure 3.7 shows the actual mounting of the sample. The issue with this proposed method is that the conductive adhesive is not very conductive at all. A multimeter verified that the adhesive layer prevented good electrical contact form being made. Another problem with the copper tape was that it was pulling up on the metal contacts and not sticking flush to the sample surface.

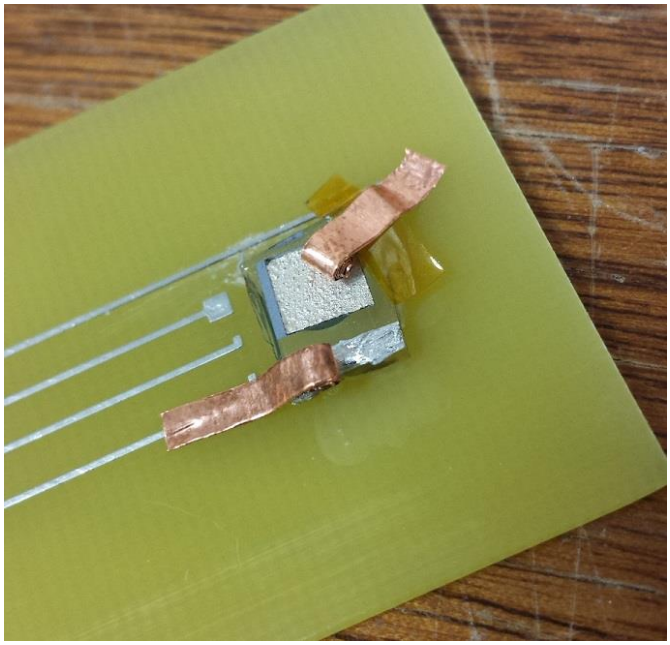

Figure 3.7: Sample preparation

The first solution to this mounting problem was to roll the copper tape on itself and then use Scotch tape to keep pressure on the contacts and ensure good electrical contact. The other end of the copper tape leads were then soldered to the PCB leads. This resulted in a crude, but effective mounting system.

A more refined mounting method will be used on the other samples. Conductive paint was acquired from Bare Conductive, a company based out of the UK. This paint was graphite based, so it would not interfere with the EDMR signal. The copper tape leads will be soldered again to the PCB leads, but this time the conductive paint will be used to fix the copper tape in place on the metal solar cell contacts as well as ensuring

good electrical contact is made. This method will minimize damage to solar cell contacts and the device itself.

Sample Holder

The sample holder was specifically designed to work with the Helmholtz coil design. The holder was designed in Autodesk Inventor Professional 2014, and then 3D printed at the Learning Factory's facilities at Penn State University.

The magnet consists of a set of nested coils, and the most uniform magnetic field is produced by the coils directly at the center of the coils' axis of symmetry. Thus, the sample holder was designed so that the cell would be in this exact spot. Other design criteria were that the sample had to be fixed and stable yet be able to be quickly removed; that the holder had to have space for RF coil to sit over the sample; and that the sample holder had to be sturdy yet cost-effective.

Many different ideas and designs were modeled in Inventor and then refined. Some of the initial designs can be shown in Figure 3.8.

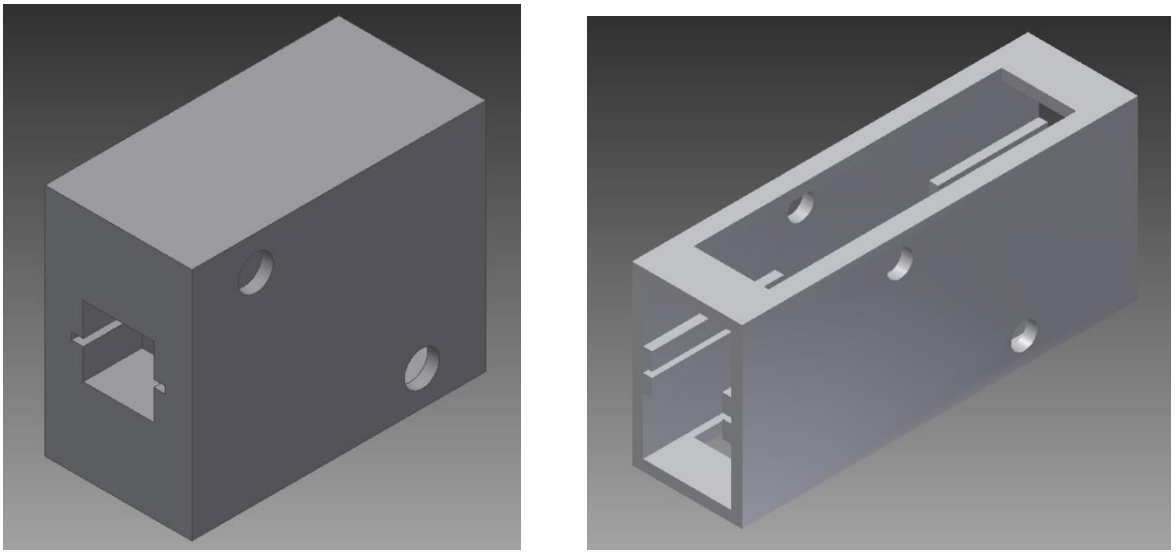

Figure 3.8: Early jig designs

The whole model was scrapped several times and restarted from scratch to ensure that the final product was sufficiently optimized. The final model featured a rail/slot system the PCB could slide in and out of, a platform for the RF coil, and an open frame design to save material costs and allow the operator a view of the sample. Thicker side walls were used to ensure that the jig was more resistant to higher temperatures if the magnet was run for extended period of time. The final design is show below in Figure 3.9.

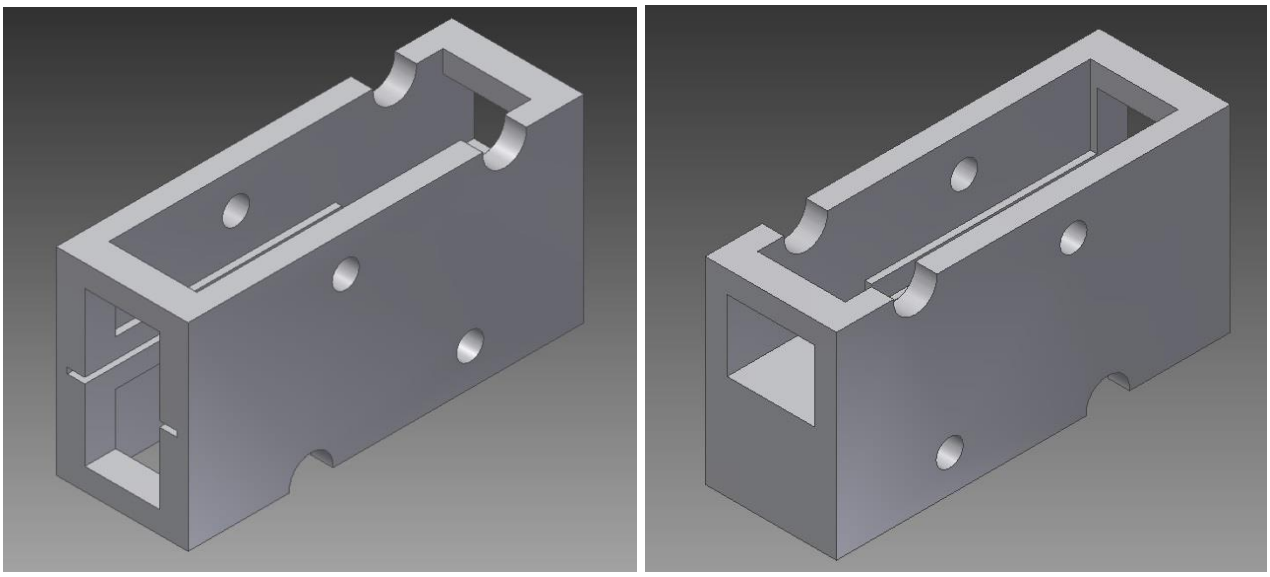

Figure 3.9: Final jig design, front (left) and back (right)

Sample Biasing

CdTe/CdS solar cells are essentially large area p-n junction diodes. Without incident light, biasing is necessary for the device to generate a current. When the device is forward biased a large current flows; a very small current flows with reverse bias. The dark current at modest forward bias can be attributed to recombination effects, so biasing

with a specific voltage will give the best results. Sample biasing was done using a homemade biasing box. The biasing box was originally designed for MOSFETs, so it has the capabilities to apply a voltage across the source, drain, or gate. This voltage is supplied by two 9 Volt batteries and can be varied using the built-in potentiometers. The solar cells had to be forward biased, so this was done by applying a voltage across the two leads connected to the device contacts.

The precise biasing voltage is very important. Biasing above the built-in voltage yields no signal. This is because for in the dark current measurements, we are measuring recombination current in the depletion region. Above the built-in voltage there is no depletion region. The recombination current is a maximum slightly below the built-in voltage. Dr. Corey Cochrane has characterized SDR signal amplitude relative to biasing voltage, and there is a narrow band where optimal signal is achieved [24].

Signal Amplification

Signal optimization is one of the most important objectives of our experimental design. The signal response from the solar cell under resonance is small and can easily be lost in noise. The output signal from the solar cell is a current, which then goes into a preamp and then a lock-in amplifier before finally going to the signal averager.

The signal from the device first passes through a current preamp. The current preamp takes the current and converts it to a voltage. The preamp has capabilities for AC and DC voltage outputs, as well as variable amplification. The gain of the current preamplifier must be chosen carefully. The signal can saturate, causing problems with

signal averaging. The current pre-amplifier also has band pass filters. These can be used to filter out unwanted frequencies in the signal. After the signal is amplified, it runs through another BNC cable into the lock-in amplifier.

Optimizing the lock-in amplifier settings is key to having high signal to noise ratios. The lock-in is phase and frequency sensitive. In a perfect system, the EDMR response would be exactly in phase with the modulation coil voltage. However, due to various capacitances and inductances in the system, the actual signal is almost inevitably out of phase of the modulation voltage. This phase shift must be taken into account to achieve the best signal amplitude.

Using its exceptional sensitivity to essentially only one specific frequency and its ability to provide phase sensitive detection, the lock-in produces a very large enhancement in our system sensitivity.

Signal Averaging

The amplified and filtered signal is then output from the lock-in amplifier and input via BNC cable to an EG&G Princeton Applied Research signal averager with display. The signal averager takes the signal input, which is in volts, and plots it on the display versus time. The time correlates directly to the magnitude of the magnetic field, so features in the EDMR spectra can be analyzed.

There are several parameters and settings to optimize on the signal averager to get better results. The first setting is “dwell time”. The dwell time setting changes the time per division of the trace, and ultimately sets the time for each run. There are 10 divisions

that make up a trace, so a dwell time of 7.168 sec/div dives a trace time of 71.68 seconds. The actual run time is slightly longer than 71.68 seconds, however. This is due mostly to the operation of the system. There is some inherent time for the system to finish a run and reset the trigger, where no data is being collected or displayed. This effectively limits the upper limit of magnetic field, and creates a slightly asymmetrical sweep. However, this effect is not very significant.

The second setting is the averaging type. The setting used was standard averaging. This setting averaged each data point over the course of a specified number of runs. The averaging could significantly reduce the signal noise. The signal noise ratio is reduced by the square root of the number of runs. Each run took anywhere from a minute to two minutes. Since the improvement scales with the square root of the number of repetitions, detection of a signal after only a few runs was important.

RF Power

The radiofrequency (RF) coil provides an electromagnetic field operating at the RF circuit's resonance frequency. The coil used is a Doty 350 MHz coil. The RF system is just a high quality factor LRC circuit with impedance matching. The Doty coil is optimized to have a sharp resonance state at precisely 350 MHz. In practice, the resonance frequency was 353 MHz. Alternate homemade RF circuits and coils were made and tested, but did not perform well enough to be used.

The important factor for a suitable RF coil is the quality factor, or Q factor. The ideal coil and circuit will have a very low signal at all frequencies except at its resonance

frequency, where it would have a sharp increase in signal amplitude. This is so because only at resonance will the coil produce strong oscillating magnetic field to the sample. The oscillating field generates the resonance response we observe in EDMR. The Q factor is a way to determine how effectively the RF circuit can be tuned to optimize the oscillating field. The Q can be measured using a secondary coil connected to an oscilloscope.

To experimentally evaluate Q, one measures the resonance frequency at which the peak occurs and then also measures the frequency at which the signal drops by 3dB, as shown in Figure 3.10. 3dB equates to log(3) which is 0.477. This means that the f_1 and f_2 frequency measurements are made when the amplitude drops by 47.7%, or about 50%.

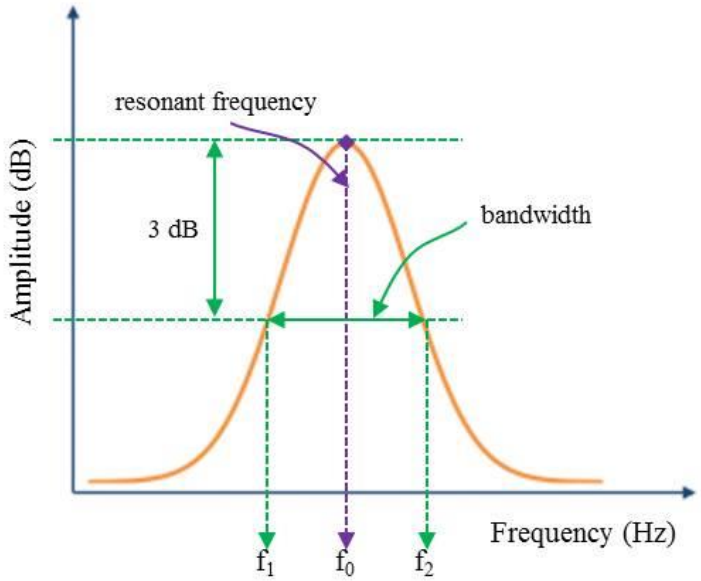

Figure 3.10: Qualitative diagram for calculating Q

Several homemade RF coils were tested, with resonance frequencies of 168 MHz, 175 MHz, and 354 MHz. However, the Q for these coils ranged from 2, 3.4, and 7.2

respectively, which was not good enough to use for our system. We decided to use a manufactured RF coil from Doty Scientific. This coil had an accompanying tuner circuit, and had a resonance condition at 353 MHz.

The Doty coil had a slightly asymmetrical drop off, with 47.7% reduction in amplitude occurring at 350 MHz and 360 MHz. The coil, as expected, gave a much better Q, with a Q equaling 35.2. This RF coil was sufficiently optimized and suitable for getting a good EDMR signal.

Chapter 4

Results

In order to test the low-field characteristics of the CdTe devices, the solar cell samples were first checked for functionality, and then the low-field EDMR system was optimized using a DMOS device that had known characteristics. The CdTe I-V characteristics will be discussed, followed by EDMR results using the DMOS device.

CdTe/CdS I-V Curve

To test that the mounting of the solar cell had been successful, a semiconductor parameter analyzer (SPA) was used. Using a Windows Basic code shown in Appendix A, the SPA could sweep over different biasing voltages and recorded the current output

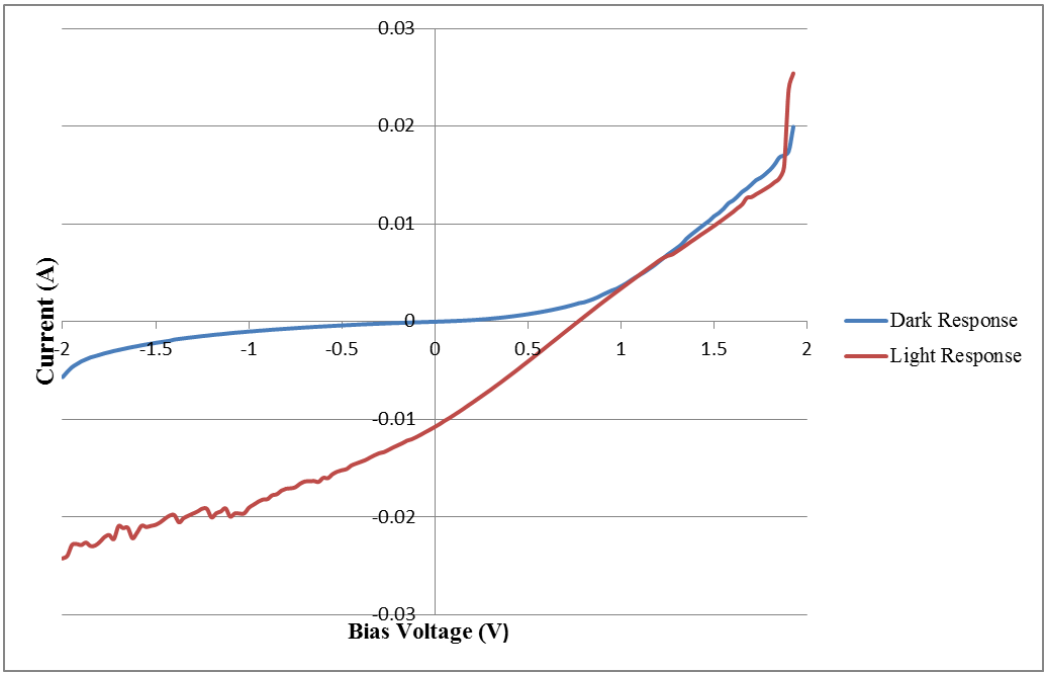

Figure 4.1: I-V curve characteristics for CdTe/CdS sample

of the device. The resulting curves are shown in Figure 4.1. The blue curve shows the I-V characteristics in the dark, while the red shows I-V characteristics under intense light from an LED flashlight. Qualitatively, the I-V characteristics indicate that the solar cell functioned correctly.

4H SiC DMOSFET Low-field EDMR Results

The DMOS device was a functional SiC transistor. This transistor was used to test the zero-field capabilities of the EDMR rig. In zero-field studies, there is no RF power used, so the result should be a current response at 0 Gauss during a magnetic field sweep. Not having RF simplifies the system, and allows for optimization without extra unknowns. For the zero-field sweep, we usually swept through either ±150 Gauss or ±75 Gauss. The various settings for these sweeps and others are tabulated in Appendix B.

Our first confirmation that we had a working system is shown in Figure 4.2. The system that recorded this result did not have either a mod box or audio amplifier. This was the result after the signal averager averaged 182 runs. There was a distinct signal close to 0 Gauss, which definitely confirmed that the system was working. However, the signal-to-noise ratio was not good, and further optimization was needed.

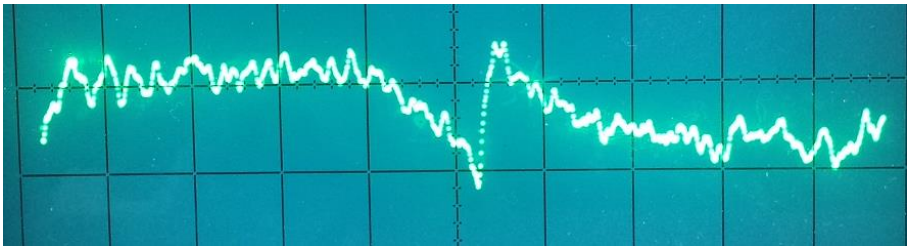

Figure 4.2: First characteristic spectra

To optimize the system further, the modulation Helmholtz coil system had to be greatly refined. In order to accomplish this, a mod box and audio amplifier were used. This helped increase the signal and decrease the noise, and we were able to get the trace in Figure 4.3 after only 25 runs.

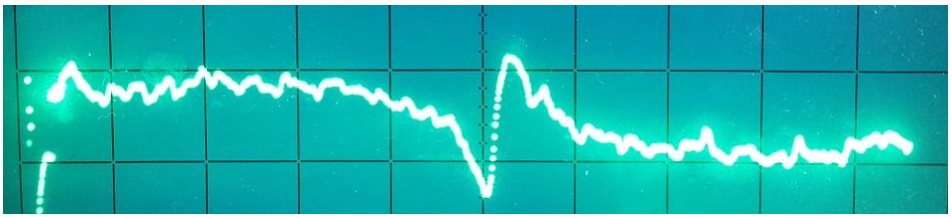

Figure 4.3: Spectra after further system optimization

Despite a better signal to noise ratio and a larger signal, the system was still not optimized. The modulation circuit was losing a lot of power, likely due to the aluminum plates around the mod coils, and as a result the system was undermodulated. The solution was to increase the mod signal amplitude significantly, to about 6 Vpp compared to 0.5 Vpp. This worked much better, and the signal was clear after just 1 run.

In addition, the system was operating well out of phase. In order to get it in phase, the phase was changed until there was almost no signal, i.e. the system was out of

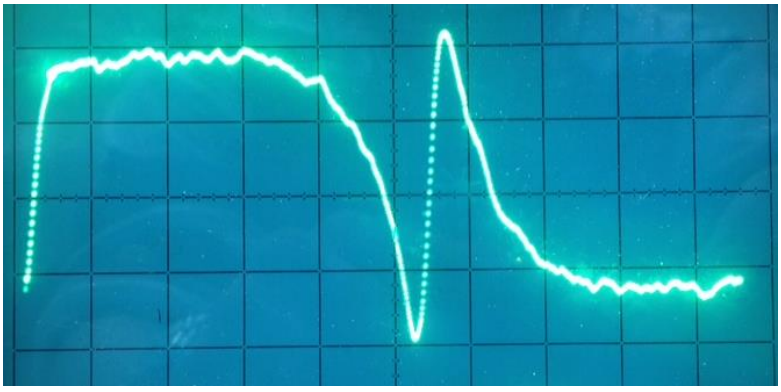

Figure 4.4: Fully optimized signal response

phase. The phase we were using was +90°, but the signal was canceled out at +40°. This means that we were losing about half of the signal amplitude. As a result, the lock-in settings were changed to +130°, and the signal amplitude was improved.

Figure 4.4 shows the EDMR spectra after the mod system was optimized. At both low and higher frequencies, the signal to noise ratio was significantly better, and it took far less time to achieve better results. The trace in Figure 4.4 took only four runs, and there is little noise, and a much better signal resolution.

CdTe/CdS Low-field EDMR Results

After numerous attempts to achieve a good signal, we achieved what could be a zero-field response. This was under high mod, and very low frequency, 75Hz. After 76 scans, the response can be seen in Figure 4.5. It would make sense the signal is broad, and the signal seems to be centered as expected at the center. However, this signal could also be a baseline of noise.

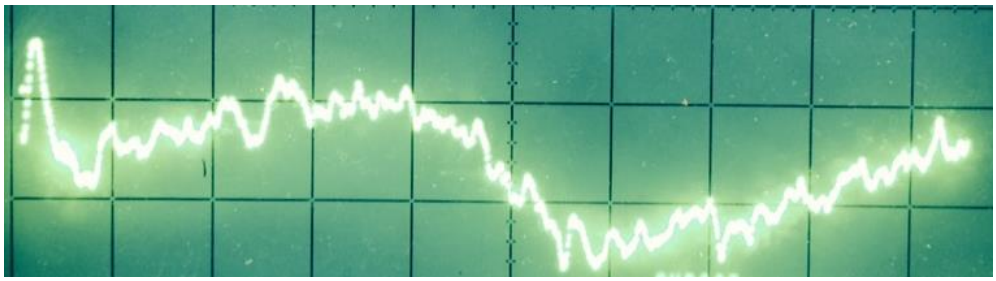

Figure 4.5: Possible CdTe/CdS zero-field response at 75Hz

After this response was achieved, the system was slightly modified. The mod box was changed to have a second resistor in parallel to prevent the components from

overheating and prevent the mod coil wire from overheating. After leaving the solar cell running for 167 scans at 100 Hz, a spectrum was achieved that can be seen in Figure 4.6.

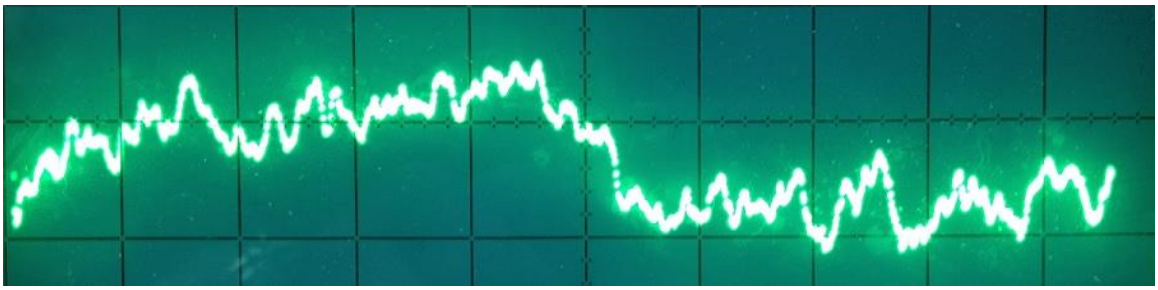

Figure 4.6: Possible CdTe/CdS zero field response at 100Hz

After zooming in on the scan, the response in Figure 4.7 looks to be convincingly like a real zero-field response. Upon closer examination, there even appear to be small features within the signal. With this much signal noise, we cannot confirm that this is a

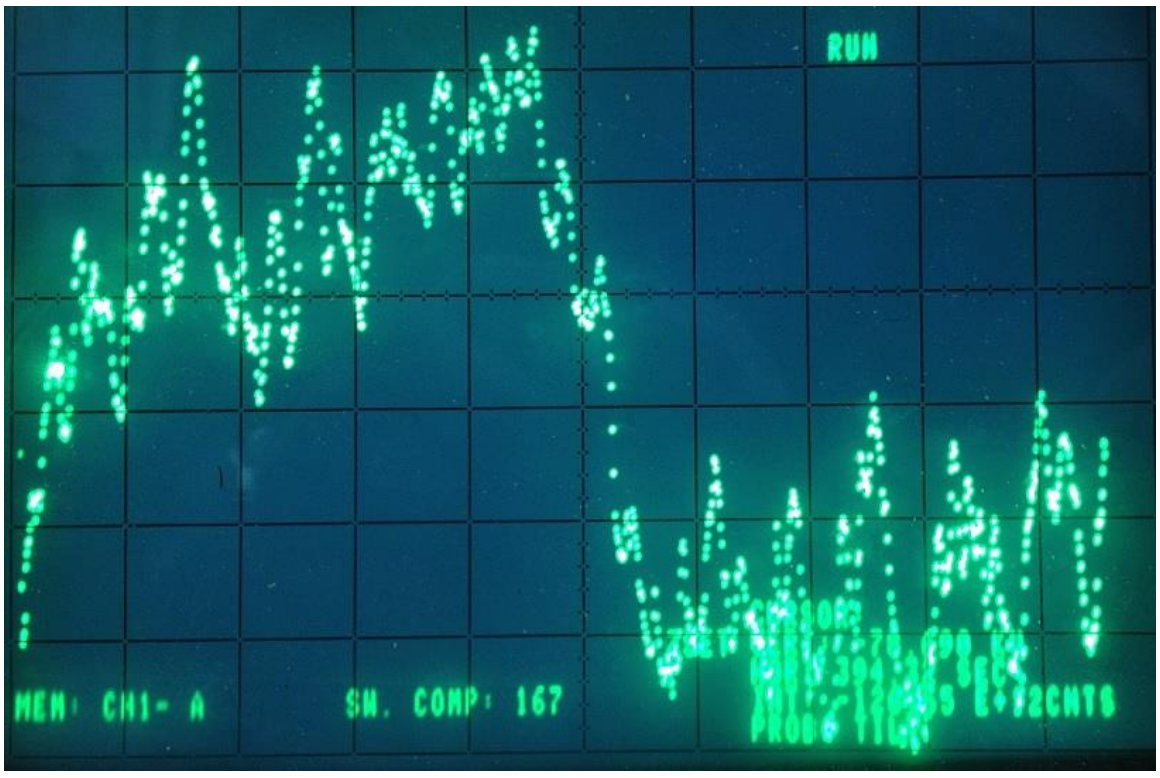

Figure 4.7: Zoomed in CdTe/CdS response at 100Hz

zero-field signal. However, it is very likely that this will become a clearer, higher signal to noise signal after the system is further modified. This will be especially the case once software can be used to further reduce signal noise.

We have successfully achieved a zero-field response for a 4H SiC DMOSFET sample, which has a known, large signal. Using this sample, we were able to optimize settings on the lock-in, including the time constant and phase. We were also able to discover and solve problems with the modulation field coils. After optimization, the signal to noise ratio improved dramatically. With optimized settings, we attempted to run a CdTe/CdS sample from NREL to achieve a zero field response. While we achieved a characteristic shape, we were unable to conclude that the response was real and not a noise floor.

Chapter 5

Discussion

We have built low-field EDMR system which is fully functional and capable of achieving an excellent signal to noise ratio. However, we have yet to implement one more step, which will make the spectrometer a research quality instrument. We will add a computer for direct data collection and control of the magnetic field. The system will output a spectrum directly comparing signal intensity to magnetic field. This allows for accurate interpretation of line-width, zero-crossing g values, and determining which defect is giving the response. Having a system that outputs signal intensity versus time can still provide useable data, but of limited precision.

Problems Encountered

There were many problems encountered with sample mounting, set-up, and system optimization. Mounting the samples was difficult because the cell had exposed soft metal contacts of indium and silver. These contacts could easily be damaged, so finding a way to mount the samples and achieve good contact was a challenge. The copper tape that Dr. Albin sent was not able to make good contact using it as was intended. This was because the adhesive would pull up and prevent good contact from being made. The adhesive was also determined to have insulating properties. To adjust for this, the copper tape was rolled on itself to provide a conducting surface and then tape

was used to apply spring tension to the copper tape. This did work, however multiple times the tape had to be reapplied because the copper had lost contact with device. An alternative method was to apply a conductive paste or paint to form an electrical connection between the cell contact and the copper tape. The conductive paint that will be used was obtained from Bare Conductive. Once applied, the paint should form a much more stable and permanent contact.

There were many problems encountered with the set-up, mainly attributed to learning how each individual system worked and becoming familiar with each piece of equipment. The first problem was figuring out how to program the power supply to ramp up in current. With no computer to input a signal, an arbitrary waveform generator had to be used to create a ramp waveform. This proved to work and be reliable, however the rapid jump the power supply made flipping current from positive to negative through the coils caused artifacts to appear on the left side of the spectra. For zero-field studies, this effect does not affect the zero field response, however adding the RF power may cause important features at the edges of the magnetic field scan to become distorted.

Another problem with the set-up was developing a useable RF coil and circuit. The Doty Scientific coil was in use for another system, so continuously swapping parts from a working system has productivity limits. An attempt was made to produce a homemade RF circuit and coil. The coils used were one and a half turns and sized to fit over the solar cell devices to apply a uniform field. With the available components, a RF circuit was created that had a Q of 7.2. This was too low and not optimized enough to be used. The likely problems were the components being used and some of the soldering required. Errant soldering and the method used to connect components on the circuit

board base could have created stray capacitances and inductances, which can significantly limit the Q. Stray capacitances can cause asymmetry at the resonance condition, which was observed during testing.

There were several problems encountered with signal processing. Most of these problems were due to unknown causes of power dissipation in the mod system. Originally, the mod coils were just powered using the built in function generator from the lock-in. However, it was clear that the system was being very undermodulated. In order to improve the signal amplitude, more current had to be run through the coils. This was done using a 1Ω circuit and an audio amplifier. The resulting signal was large enough to modulate at a more optimal field width. Although there is some uncertainty regarding where the large power loss is coming from, the aluminum plates forming the mod coils may be causing some power dissipation.

The other issue was in amplification. Figure 5.1 shows the signal response using two different pre-amps. Using the same set-up and lock in settings, just switching pre-

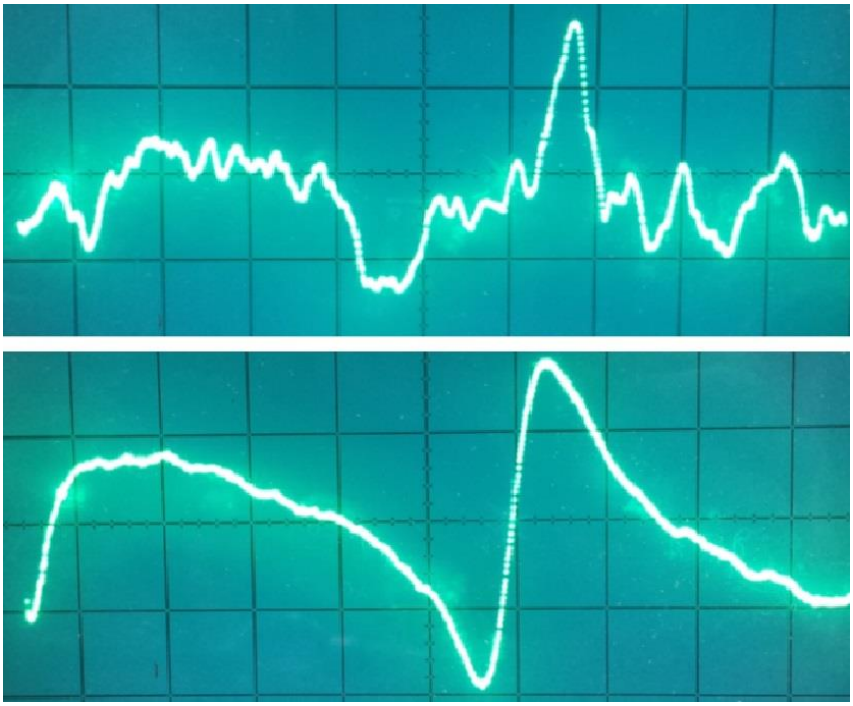

Figure 5.1: Comparison of signal response using two different current pre-amps

amps, gave two very different results. The top spectrum was recorded using a Signal Recovery Model 5182 pre-amp after ten runs. The lower signal was obtained using a SRS pre-amp after just two runs. We initially wanted to switch over to the Signal Recovery pre-amp in order for an EPR system to be re-built with the SRS pre-amp, however, there are unknown issues with the SRS that must be first addressed.

It is clear that the Signal Recovery pre-amp has much more noise. There is a peak in a similar location, indicating that there is a signal, but the resolution is too low. One possible explanation is that the SRS pre-amp has high and low-pass filters. The extra noise could be extraneous signals at high or low frequencies. The modulation frequency was low and in the correct operating range for the pre-amp as verified from the manual.

Future Work

While much of the EDMR system developed was composed of newer, high-quality equipment, some of the important components were outdated. By using a computer-based setup, the lock-in amplifier, signal averager, and arbitrary waveform generator can be removed. Instead, software developed by Dr. Corey Cochrane can be used to control the power supply, act as a virtual lock-in, and record the data. In addition, the software has built-in noise reduction algorithms. A computer-based system would be ideal for future research, and would provide more detailed EDMR spectra and more accurate results.

Future research areas for the CdTe solar cells include recording EDMR results using sub-bandgap photon excitation. Using LED lasers with varying wavelengths

corresponding to possible deep level defects could give a more detailed account of defect centers and the corresponding sources.

Appendix A
Calculations & Programs

Windows basic code used for I-V curves:

```
config HP4145:03 RANGE:0
!
! SMU1 -> GATE; SMU2(red) -> DRAIN; SMU3 -> Source(yellow); SMU4 ->
Bulk(green)
!
WAIT
! NO LIGHT
!
sweep0 i=1 L=0.1 s4(-2;0.025;2) v4=0 YL=-8 Y=0 M4 M2 o=4
!
WAIT
! WITH LIGHT
!
sweep0 i=1 L=0.1 s4(-2;0.025;2) v4=0 YL=-8 Y=0 M4 M2 o=1
BEEP
BEEP
BEEP
!
End
```

This code runs two I-V curves. The first, as indicated, is in the dark, and the second is under light. The sweep was from -2 to 2 Volts at 0.025 Volt increments. The output plot was shown with a log scale. The data was imported in Excel and the resulting I-V curve is shown in Figure 4.1.

Table 1: System settings at 5 Gauss mod

Scan width (Gauss)	Time constant (s)	Scan time (s)
60	0.3	18
60	1	60
75	0.3	22.5
150	0.3	45
150	1	150
300	0.3	100
300	1	300

Settings in Table 1 were established using the following equation assuming a 5 Gauss modulation field width:

$$S.T. = S.W. * \tau$$

where S.T. is the scan time of the system, scan width is the full scan field width, and τ is the time constant used for lock-in detection. Knowing that we had about a 5 Gauss modulation width allowed us to vary these settings to predictably get optimal system settings.

Appendix B
System Components

Table 2: System component details

Instrument Type:	**Manufacturer and Details:**
Arbitrary waveform generator	Fluke 291 100MS/s arbitrary waveform generator
Bipolar operational power supply	Kepco BOP 50-2M
Frequency generator	Boonton 102E FM/AM signal generator
RF coil	Doty Scientific Inc. 350 MHz remote coil matching network
Audio amplifier	Insignia AM/FM stereo receiver NS-R2001
Current pre-amp	Stanford Research Systems model SR570
Lock-in amplifier	Stanford Research Systems model SR830 DSP lock-in amplifier
Signal averager	EG&G PARC Model 4203 signal averager and EG&G PARC Model 4001 display

References

[1] C. Philibert, "The present and future use of solar thermal energy as a primary source of energy," *Int. Energy Agency, Intern. …*, pp. 1–16, 2005.

[2] W. Shockley and H. J. Queisser, "Detailed Balance Limit of Efficiency of p-n Junction Solar Cells," *J. Appl. Phys.*, vol. 32, no. 3, p. 510, 1961.

[3] "Thin Film Module Technology." [Online]. Available: http://www.firstsolar.com/en/technologies-and-capabilities/pv-modules/first-solar-series-3-black-module/cdte-technology.

[4] P. M. Lenahan, "Magnetic Resonance and Electrically Active Defects in II VI Compound Semiconductor Solar Cells," 2012.

[5] S. Van Fechtmann, "Cadmium Telluride – The Good and the Bad," 2012. [Online]. Available: http://www.solar-facts-and-advice.com/cadmium-telluride.html.

[6] V. M. Fthenakis, H. C. Kim, and E. Alsema, "Emissions from photovoltaic life cycles.," *Environ. Sci. Technol.*, vol. 42, no. 6, pp. 2168–74, Mar. 2008.

[7] F. Rong and E. Poindexter, "Electrically detected magnetic resonance in pn junction diodes," *Solid state …*, vol. 76, no. 8, pp. 1083–1086, 1990.

[8] J. R. Sites, "Thin-film photovoltaics: What are the reliability issues and where do they occur?," *2010 IEEE Int. Reliab. Phys. Symp.*, pp. 494–498, 2010.

[9] M. Pigott, L. Young, P. M. Lenahan, A. Halverson, K. W. Andreini, and B. a. Korevaar, "Electron paramagnetic resonance as a probe of technologically relevant processing effects on CdTe solar cell materials," *2013 IEEE 39th Photovolt. Spec. Conf.*, no. 1, pp. 0635–0638, Jun. 2013.

[10] I. Stefaniuka, M. Bestera, I. Virtb, and M. Kuzmaa, "EPR spectra of Cr in CdTe crystals," vol. 108, no. 2, pp. 413–418, 2005.

[11] P. Emanuelsson, P. Omling, and B. Meyer, "Identification of the cadmium vacancy in CdTe by electron paramagnetic resonance," *Phys. Rev. B*, vol. 47, no. 23, pp. 578–580, 1993.

[12] G. Brunthaler and W. Jantsch, “An A centre in CdTe,” *J. Phys. …*, vol. 1925, pp. 1–5, 1989.

[13] B. Meyer, P. Omling, E. Weigel, and G. Müller-Vogt, “F center in CdTe,” *Phys. Rev. B*, vol. 46, no. 23, pp. 135–138, 1992.

[14] P. Christmann, H. Alt, and D. Hofmann, “Optically detected magnetic resonance investigations on titanium and vanadium ions in CdTe,” *Opt. Mater. (Amst).*, vol. 4, no. January, pp. 210–213, 1995.

[15] G. Brunthaler, W. Jantsch, U. Kaufmann, and J. Schneider, “Electron-spin-resonance analysis of the deep donors lead, tin, and germanium in CdTe,” *Phys. Rev. B*, vol. 31, no. 3, pp. 1239–1243, 1985.

[16] L. C. Smith, S. J. Bingham, J. J. Davies, and D. Wolverson, “Electron paramagnetic resonance of manganese ions in CdTe detected by coherent Raman spectroscopy,” *Appl. Phys. Lett.*, vol. 87, no. 20, p. 202101, 2005.

[17] R. G. Dhere, J. N. Duenow, C. M. Dehart, J. V Li, D. Kuciauskas, and T. A. Gessert, “Development of Substrate Structure CdTe Photovoltaic Devices with Performance Exceeding 10 % Preprint,” no. August, 2012.

[18] K. Saminadayar, D. Galland, and E. Molva, “Electron paramagnetic resonance studies of chlorine, indium and aluminium-doped CdTe crystals,” *Solid State Commun.*, vol. 49, no. 7, pp. 627–630, 1984.

[19] K. Saminadayar, J. Francou, and J. Pautrat, “Electron paramagnetic resonance and photoluminescence studies of CdTe: Cl crystals submitted to heat treatment,” *J. Cryst. Growth*, vol. 72, pp. 236–241, 1985.

[20] S. Demtsu, D. Albin, J. Sites, W. Metzger, and A. Duda, “Cu-related recombination in CdS/CdTe solar cells,” *Thin Solid Films*, vol. 516, pp. 2251–2254, 2008.

[21] A. Al-Dhafiri, “Photovoltaic properties of CdTe-Cu 2 Te,” *Renew. energy*, vol. 14, pp. 101–106, 1998.

[22] S. Asher and F. Hasoon, “Determination of Cu in CdTe/CdS devices before and after accelerated stress testing,” *… Rec. …*, 2000.

[23] G. G. Scott, “Compensation of the Earth’s Magnetic Field,” *Rev. Sci. Instrum.*, vol. 28, no. 4, p. 270, 1957.

[24] C. J. Cochrane, P. M. Lenahan, and a. J. Lelis, “Deep level defects which limit current gain in 4H SiC bipolar junction transistors,” *Appl. Phys. Lett.*, vol. 90, no. 12, p. 123501, 2007.

[25] P. M. Lenahan, “A Brief Introduction to Electron Spin Resonance.”

ACADEMIC VITA OF ERIK T. SHAW

38 Cherrydale Road ◇ Glen Mills, PA 19342
(484)-844-4017 ◇ shawerikt@gmail.com

EDUCATION

The Pennsylvania State University — May 2014
Schreyer Honors College — *University Park, PA*
Bachelor of Science in Engineering Science (Honors Curriculum)
Minor in Engineering Mechanics

TECHNICAL EXPERIENCE

Penn State Semiconductor Spectroscopy Lab — August 2013 - Present
Undergraduate Research Assistant — *University Park, PA*

- Designed a low-field EDMR system capabable of analyzing quantum scale defects in electronic devices
- Analyzed recombination centers in CdTe/CdS photovoltaic cells using the low-field EDMR setup

Naval Sea Systems Command — May 2013 - August 2013
Engineering Intern — *Bremerton, WA*

- Reactor engineering intern specializing in refueling ventilation for submarines and aircraft carriers
- Provided project support using Solid Edge drafts and models to design vent systems and fittings

Engineering Design Project — September 2010 - December 2010
Team Leader — *University Park, PA*

- Developed a telecom station that uses 100% renewable energy sources and eco-friendly architecture
- Managed project schedule, design selection, and prototype construction during the entire process

LEADERSHIP EXPERIENCE

Engineers for a Sustainable World, Penn State Chapter — August 2011 - Present
Vice President — *University Park, PA*

- Won ME/NucE Innovation Competition and $2000+ to build Apparatus X, a micro living unit and workspace
- Led meetings and helped delegate tasks to officer team to increase productivity and efficiency

Penn State Alumni Association, Blue & White Society — December 2013 - Present
Treasurer — *University Park, PA*

- Oversaw a $43,000 budget and three accounts, allocating funds between the organization's different committees
- Met with executive board to plan finances for events like THON, Relay for Life, and fundraisers

Penn State Dance Marathon — October 2010 - April 2013
Volunteer, Recycling Effort Chair — *University Park, PA*

- Contributed to campus-wide recycling effort and educated members about reducing waste
- Fundraised for THON, which has raised over $114 million to help fight pediatric cancer

Schreyer Honors College Orientation — October 2011 - September 2012
Student Mentor — *University Park, PA*

- Selected to participate in mentor training, which consisted of leadership seminars and planning workshops
- Mentored over 15 incoming freshmen and assisted them with the transition to campus life

SKILLS & QUALIFICATIONS

Computer: Autodesk Inventor, Solid Edge, SolidWorks, MATLAB, Multisim, Ultiboard, LaTeX, and C++
Language: Intermediate German, basic French
Qualifications: Confidential security clearance